Origin and evolution of the multiply quantized vortex instability

Sam Patrick [1,2,*] August Geelmuyden [3,†] Sebastian Erne [3,4,‡] Carlo F. Barenghi [5,§] and Silke Weinfurtner [3,6,‖]

[1]*Department of Physics and Astronomy, University of British Columbia, Vancouver, British Columbia, Canada V6T 1Z1*
[2]*Institute of Quantum Science and Engineering, Texas A&M University, College Station, Texas 77840, USA*
[3]*School of Mathematical Sciences, University of Nottingham, University Park, Nottingham NG7 2RD, United Kingdom*
[4]*Vienna Center for Quantum Science and Technology, Atominstitut, TU Wien, Stadionallee 2, 1020 Vienna, Austria*
[5]*Joint Quantum Centre Durham-Newcastle, School of Mathematics, Statistics and Physics, Newcastle University, Newcastle upon Tyne NE1 7RU, United Kingdom*
[6]*Centre for the Mathematics and Theoretical Physics of Quantum Non-Equilibrium Systems, University of Nottingham, Nottingham NG7 2RD, United Kingdom*

(Received 24 December 2021; revised 29 March 2022; accepted 8 June 2022; published 14 November 2022)

We show that the dynamical instability of quantum vortices with more than a single unit of circulation results from a superradiant bound state inside the vortex core. We then reveal a striking behavior of the system in the nonlinear regime. Counter to the expectation that the instability should produce well-separated vortices, the system evolves into a bound state of corotating singularities orbiting within a few healing lengths of each other, undergoing modulations in separation. During these modulations, kinetic energy is traded back and forth between sound waves and vortical degrees of freedom.

DOI: 10.1103/PhysRevResearch.4.043104

I. INTRODUCTION

A striking property of quantum fluids (superfluid helium, atomic Bose-Einstein condensates, polariton condensates, etc.) is that the circulation of the velocity $\mathbf{v}$ around a closed path C is quantized [1] in units of $\kappa = 2\pi\hbar/M$,

$$\oint_C \mathbf{v} \cdot d\mathbf{r} = \ell\kappa, \tag{1}$$

where M is the boson's mass, $\hbar$ is the reduced Planck's constant, and the integer ℓ is called the winding number. In most regions of fluid the circulation will be zero, but there may be points [two-dimensional (2D)] or lines [three-dimensional (3D)] where the wave function Ψ vanishes; hence, its phase is not defined, and $\ell \neq 0$. Such topological defects (singularities), normally surrounded by circular (2D) or tubular (3D) regions of depleted density, are called quantum vortices. The topological nature of these vortices deeply affects the possible flow patterns (vortex lattices, turbulence, etc. [2–4]).

Experiments [5–7] show that a multiply quantized vortex (MQV), i.e., a vortex with $\ell > 1$, will spontaneously decay into a cluster of singly quantized vortices (SQVs), each with $\ell = 1$. This tendency is usually justified since, for a given circulation, a cluster of SQVs is energetically favorable compared with a MQV [8]. Hence, in a dissipative system which relaxes into the lowest energy state, an MQV will naturally evolve into a cluster of SQVs. In nondissipative systems, however, the decay can still occur due to a dynamical instability [9] arising from the coupling of the MQV to surrounding phonons.

The instability of MQVs acquires additional significance if we note that, under certain conditions, there are analogies between vortices and rotating black holes [10]. It has recently been argued [11] that the dynamical instability is related to the existence of an ergoregion, a notion from black hole physics which implies superradiant amplification of waves in a particular frequency range [12]. Superradiance arises not only around rotating black holes but in a wide range of systems, e.g., draining vortices [13] and optical vortex beams [14]. However, unbounded growth can occur if there is a mechanism for trapping superradiant modes in the system, eventually driving it into the nonlinear regime, e.g., black hole bomb instabilities [15].

In this paper we study the evolution of an $\ell = 2$ MQVs in a bucket trap. Our analytic Wentzel-Kramers-Brillouin (WKB) prediction confirms the superradiant character of the dynamical instability in the initial linear regime [11]. By solving the full nonlinear equations, we also reveal a remarkable recurrent behavior of the instability at later times: a modulation in which incompressible and compressible kinetic energies are periodically exchanged and the two phase singularities move in and out while rotating in close proximity. This time-dependent state is the limiting configuration of two parallel quantum vortices at close distances comparable to the healing length.

*sampatrick31@googlemail.com
†august.geelmuyden@nottingham.ac.uk
‡sebastian.erne@tuwien.ac.at
§carlo.barenghi@newcastle.ac.uk
‖silke.weinfurtner@nottingham.ac.uk

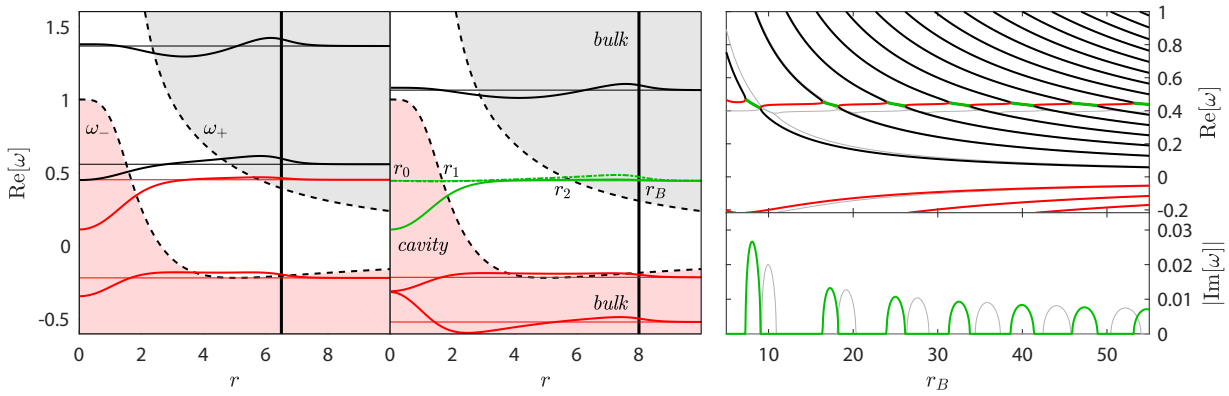

FIG. 1. Left: Oscillation frequencies and the associated eigenmodes as a function of radius. Horizontal lines are the real part of the eigenvalues Re[ω], and the superimposed thick lines are the relative density eigenmodes $\delta\rho/\rho = u_+ + u_-$, which are solutions of the BdG (5) for $m = \ell = 2$. The solid vertical line represents the trap size $r_B = 6.5$. The dashed black curves $\omega_\pm$ separate the gray (positive norm), white (evanescent), and pink (negative norm) regions. Modes with $\mathcal{N} > 0$ ($\mathcal{N} < 0$) are colored black (red). Middle: The same for $r_B = 8$. The unstable mode, whose real (imaginary) part is shown by a solid (dashed) green line, results from the coupling of two nearby modes in the left panel. The complex conjugate of this mode (not shown) is a decaying solution. Also indicated are the turning points r_i. Right: The eigenvalues ω as a function of r_B, with the real (imaginary) part in the top (bottom) panel. BdG solutions are shown as thick lines and follow the same color scheme as in the previous panels. Solutions to the WKB condition (7) are shown in gray in the background and, for high frequencies, are indistinguishable from the BdG results. WKB misses the precise location of the stability windows since the cavity mode frequency is consistently underestimated due to ρ varying quickly in the core.

II. VORTEX STATES

We consider the dimensionless two-dimensional Gross-Pitaevskii equation (GPE) for the mean-field condensate wave function Ψ,

$$i\partial_t \Psi = \left[-\tfrac{1}{2}\nabla^2 + V(\mathbf{x}) - 1 + |\Psi|^2 \right]\Psi, \tag{2}$$

where lengths are measured in units of $\xi \equiv \hbar/\sqrt{M\mu}$ (the healing length), time is in units of $\tau \equiv \hbar/\mu$, and density $|\Psi|^2$ is in units of μ/g. Note that the healing is sometimes defined with a factor of $\sqrt{2}$ on the denominator; however, this only rescales our spatial coordinate axis and does not affect the results. Here, μ is the chemical potential, M is the atomic mass, and $g > 0$ is the 2D interaction strength. We work in polar coordinates $\mathbf{x} = (r, \theta)$. The condensate is confined by a circular bucket potential of the form

$$V(r) = \frac{V_0}{1 + (V_0 - 1)e^{a(r_B - r)}}, \tag{3}$$

where r_B is the trap size and V_0 and a determine the steepness of the bucket wall at r_B. We choose $a = V_0 = 5$, although our results are essentially independent of this choice provided the wall at r_B is steep.

Using the Madelung representation $\Psi = \sqrt{\rho}e^{i\Phi}$, the stationary GPE has vortex solutions with velocity $\mathbf{v} \equiv \nabla\Phi = \ell/r\,\hat{\mathbf{e}}_\theta$, where ∇ is the 2D gradient operator. Here we focus on the doubly winded vortex with $\ell = 2$. The corresponding density ρ can then be obtained by substituting $\Phi = \ell\theta$ in (2) and solving numerically.

III. LINEAR DYNAMICS

Since $V(\mathbf{x})$ is independent of t and θ, linear fluctuations $\delta\psi$ of the condensate wave function can be decomposed into frequency ω and azimuthal m components,

$$\begin{pmatrix} \delta\psi \\ \delta\psi^* \end{pmatrix} = \int_{-\infty}^{\infty} \frac{d\omega}{2\pi} \sum_{m=-\infty}^{\infty} e^{im\theta - i\omega t} \begin{pmatrix} u_+ e^{+i\ell\theta - it} \\ u_- e^{-i\ell\theta + it} \end{pmatrix}, \tag{4}$$

where we write $u_\pm = u_\pm(\omega, m, r)$ for brevity. The fluctuations can then be described by $|U\rangle = (u_+, u_-)^{\mathrm{T}}$, which obeys the Bogoliubov–de Gennes (BdG) equation [16],

$$\widehat{L}|U\rangle = \omega|U\rangle, \quad \widehat{L} = \begin{pmatrix} D_+ & \rho \\ -\rho & -D_- \end{pmatrix},$$
$$D_\pm = -\frac{1}{2}\left[\partial_r^2 + \frac{1}{r}\partial_r - \frac{(m \pm \ell)^2}{r^2}\right] + V(r) + 2\rho - 1. \tag{5}$$

The BdG conserves the norm,

$$\mathcal{N} = \int d^2\mathbf{x}(|u_+|^2 - |u_-|^2), \tag{6}$$

which is related to the mode energy by a factor of ω. Solutions to (5) are obtained by diagonalizing $\widehat{L}$ to obtain the eigenvalues ω and eigenfunctions $|U\rangle$. In Fig. 1, we show examples of the $m = 2$ relative density eigenfunctions $\delta\rho/\rho = u_+ + u_-$ for $r_B = 6.5$ (left panel) and $r_B = 8$ (middle panel). In the right panel we display the spectrum of eigenvalues ω as a function of r_B, indicating with color the sign of $\mathcal{N}$. The instability (a zero-norm solution) results from the coupling of a positive-norm mode to a negative-norm one, which (for $\ell = 2$) occurs only for $m = 2$. For particular system sizes, this coupling is suppressed, and the instability is absent. In the limit that $r_B \to \infty$, the density of $\mathcal{N} > 0$ states becomes a continuum, and the coupling always occurs [11]. Note that the unstable growing mode (Im[ω] > 0) is accompanied by its complex conjugate, which corresponds to a stable decaying mode (Im[ω] < 0).

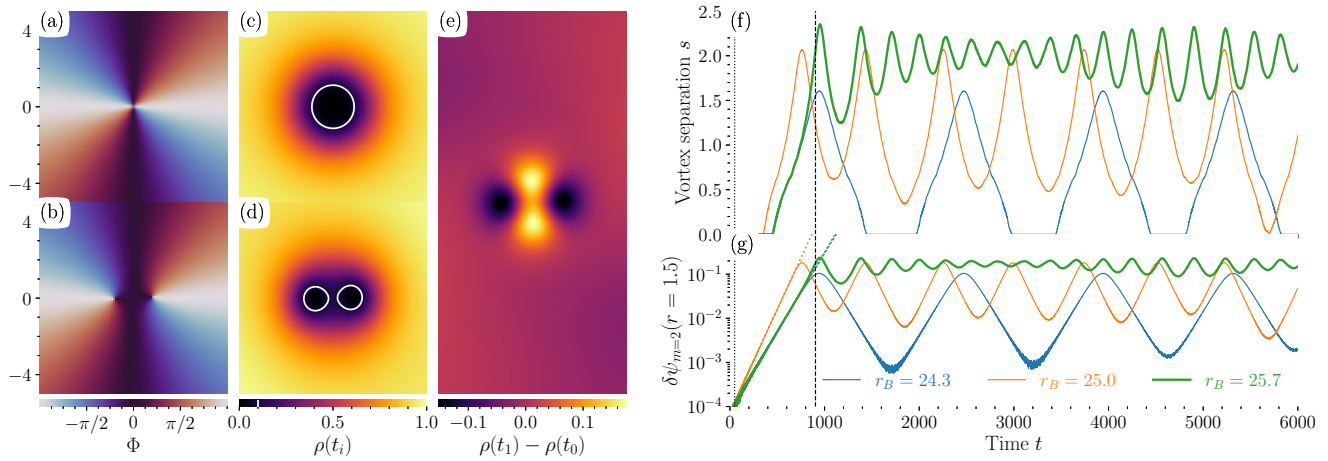

FIG. 2. The splitting of the initial MQV into two singularities. (a) and (b) show the phase Φ for $r_B = 25$ at $t_0 = 50$ and $t_1 = 904$, respectively. (c) and (d) display the density ρ at the same times; white lines are surfaces of $\rho = 1/10$. (e) displays the difference between ρ at t_0 in (c) and the density at t_1 in (d): there is a dominant $m = 2$ mode whose troughs coincide with the locations of the phase singularities $\mathbf{x}_1$ and $\mathbf{x}_2$. The x and y ranges are $[-5, 5]$ for (a)–(d), and the y range is doubled for (e). The separation $s = |\mathbf{x}_1 - \mathbf{x}_2|$ between the two phase singularities is shown to oscillate with t in (f) for three different values of the trap size r_B. Finally, (g) shows the time evolution of the $m = 2$ mode amplitude inside the cavity. The initial growth rates agree with the prediction of our linear analysis (dotted lines). Note that the blue and green dotted lines are essentially overlapping since the growth rates are the same. During the nonlinear evolution ($t \gtrsim 1000$) the amplitude is modulated in a trap-size-dependent manner.

Further insight into the spectrum can be obtained using the WKB method [17], wherein fluctuations are assumed to behave locally like plane waves on a smoothly varying background. The method (elucidated in our companion paper [18]) defines two curves $\omega_\pm(r)$ which separate the (r, ω) space into regions of positive and negative norm density, as shown in the left and middle panels of Fig. 1. Since the total norm is conserved, superradiant amplification occurs when a given ω mode tunnels from a region of positive norm to one with negative norm, i.e., from above ω_+ to below ω_-. Instabilities arise when superradiant modes become trapped. This occurs for vortices since there is reflection at the vortex axis $r = 0$ and, in the presence of a trapping potential, also at $r = r_B$. In the WKB approximation, the eigenvalue equation for modes which tunnel from above ω_+ to below ω_- is

$$4\cot(S_{01})\cot(S_{2B} + \pi/4) = \exp(-2S_{12}). \tag{7}$$

$S_{ij}(\omega) = \int_{r_i}^{r_j} |p(\omega)| dr$ is the phase integral between the turning points r_i, indicated on Fig. 1. p solves the dispersion relation $\Omega^2 = \rho k^2 + \frac{1}{4}k^4$, with $k^2 = p^2 + (m^2 + \ell^2)/r^2 + 2(\rho + V - 1)$ being an effective wave number and $\Omega = \omega - m\ell/r^2$ being the frequency in the fluid frame (see [18] for details). Solutions to (7) are shown in light gray in the right panel of Fig. 1 and clearly capture all the features of the spectrum obtained from numerical evaluation of the BdG.

The condition (7) has three types of solutions. Modes which occupy the cavity centered around the vortex core satisfy $\cot S_{01} \simeq 0$, e.g., the mode with $\omega > 0$ and $\mathcal{N} < 0$ in Fig. 1 (right panel). All the other real eigenvalues in this plot are phonons in the bulk of the condensate which obey $\cot(S_{2B} + \pi/4) \simeq 0$. Complex-conjugate pairs of eigenvalues (one of which is an instability) occur when the cavity mode couples to a phonon, such that only the product of the two cotangent functions is exponentially small. In the limit that $r_B \to \infty$, (7) reduces to

$$\cot S_{01}(\mathrm{Re}[\omega]) = 0, \quad \mathrm{Im}[\omega] = -\frac{\log|\mathcal{R}|}{2\partial_\omega S_{01}}\bigg|_{\mathrm{Re}[\omega]}, \tag{8}$$

where $|\mathcal{R}| = (1 + e^{-2S_{12}}/4)/(1 - e^{-2S_{12}}/4)$ is the local reflection coefficient associated with the tunneling between the bulk and the cavity. The factor in the denominator is negative since the cavity modes have negative norm density. Hence, we see that the origin of the instability is superradiant amplification, namely, $|\mathcal{R}| > 1$ [12].

IV. NONLINEAR DYNAMICS

To investigate the nonlinear evolution of the instability, we numerically evolve the GPE (2) for an $\ell = 2$ vortex (see Appendix A for details). We observe that the initial $\ell = 2$ phase singularity splits into two $\ell = 1$ singularities, as shown in Figs. 2(a)–2(d) for $r_B = 25$, each guided by a trough of the unstable $m = 2$ mode [Fig. 2(e)]. The separation between the two singularities varies in accordance with the amplitude of the $m = 2$ mode, as illustrated in Figs. 2(f) and 2(g) for three different r_B. Figure 2(g) also shows that the instability predicted by the linear analysis agrees with the full numerics for $t \lesssim 1000$ [19] online.

Surprisingly, we find that once the separation between the singularities reaches approximately two or three healing lengths, they begin to spiral back inwards. Since both singularities occupy the same region of depleted density, they cannot be referred to as separate vortices, as this would imply a singularity embedded in its own low-density region (the vortex core). During the inward stage, the $m = 2$ wave form matches that of the linear decaying mode (which is the complex conjugate of the unstable mode). This mode describes the reabsorption of a phonon by the pair of singularities. Eventually, growth resumes, causing a modulation of the pair

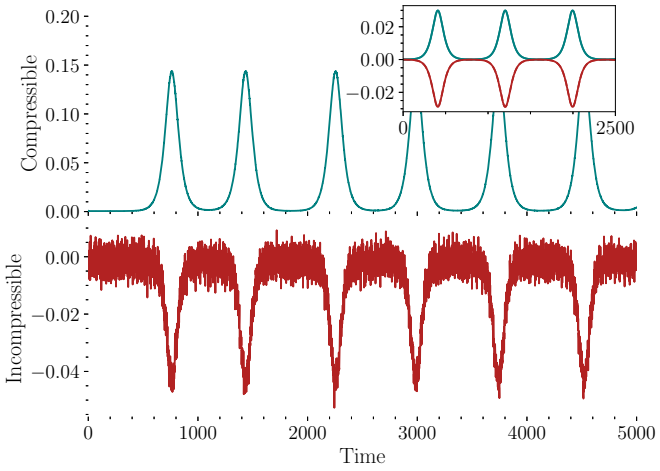

FIG. 3. Time evolution of the compressible (green line) and incompressible (red line) kinetic energies associated with phonons and phase singularities, respectively. The correlation between increases (decreases) in compressible (incompressible) kinetic energy supports our interpretation that the observed modulations are driven by an energy exchange between singularities and phonons. The inset shows the energies, i.e., H_+ (green line) and H_- (red line), of our simple oscillator model described in Appendix C for $\Omega = 1$, $\sigma = 1/50$, $g = 1/200$, $c_+ = 0$, and $c_- = 2$. This captures the behavior seen in our simulations.

separation. This cycle repeats, in a manner sensitive to the trap size, for the duration of our simulations [see Fig. 2(f)]. These modulations are driven by the exchange of energy between phonons and phase singularities. Indeed, in Fig. 3 we display the compressible (phonon) and incompressible (containing the singularities) kinetic energies [20], finding that when the former increases, the latter decreases.

In Appendix C we describe a simple dynamical system consisting of two oscillators $\mathbf{X}_\pm$ with opposite-sign energies $H_\pm = \pm(\frac{1}{2}\dot{\mathbf{X}}_\pm^2 + V_\pm)$, which describes the essential interaction between phonons and phase singularities. The potential and interaction energies are $V_\pm = \frac{1}{2}(\Omega^2 \pm \sigma)\mathbf{X}_\pm^2 - \frac{1}{4}c_\pm \mathbf{X}_\pm^4$ and $V_{\rm int} = g\mathbf{X}_+ \cdot \mathbf{X}_-$. We show how this system can be solved in the limit of large Ω to reveal the signature switch between exponential growth and decay seen in our simulations, as shown in the inset of Fig. 3. The characteristic feature which allows this is that the negative-energy cavity mode (which results in the formation of two singularities) couples only to a single phonon in the bulk, and couplings to all other phonons are considered negligible.

The physical mechanism underpinning this behavior is captured by the following argument. While the instability is growing, the nonlinearity in the GPE reduces the frequency of the cavity mode until it can no longer couple to the phonon that rendered it unstable. After decoupling, the phonon will oscillate faster than the cavity mode, and the phase difference between the two will change. Upon recoupling, this accumulated phase difference results in the complex conjugate of the unstable mode, i.e., the decaying mode. For this argument to hold, the density of phonon states in Fig. 1 must be sufficiently low that the cavity mode cannot couple to any phonons of lower frequency as it evolves. Hence, we would not expect modulations of the pair separation to occur in a very large system where the density of phonon states is effectively continuous. This being said, we have found that modulations can persist for trap sizes up to at least $r_B = 47$.

In addition to the two singularities remaining confined inside the same region of suppressed density, as shown in Fig. 2(d), the maximum value of the density perturbation $|\delta\Psi|$ during the evolution is only about 0.2. This suggests that the full nonlinear dynamics can, indeed, be described perturbatively about the original $\ell = 2$ vortex background, in contrast to the expectation that a MQV should decay nonperturbatively into a cluster of well-separated SQVs. One might assume that this behavior is highly sensitive to initial conditions and that any small perturbation might be enough to destroy the effect. While this seems to be the case when the vortex is placed far from the center of the trap [7], we have found that our modulations persist even if the vortex is displaced from the origin by a few healing lengths. We have also checked what happens when damping is added to the dynamics. Energy is then slowly removed from the system, forcing the singularities to eventually separate into vortices which obey Hamiltonian vortex dynamics [21]. Before this, however, the cavity mode (whose frequency decreases monotonically) will couple to any available lower-frequency phonons, causing modulations of the vortex separation as the singularities gradually drift apart (see Appendix B for an example). Hence, we expect the modulations will have observable consequences in real experiments where dissipation is important.

V. CONCLUSION

We have studied the instability of a doubly quantized $\ell = 2$ vortex using three distinct methods: a linear BdG stability analysis, a WKB approximation, and a fully nonlinear numerical simulation of the GPE. The WKB method allowed us to identify the cause of the instability as a superradiant bound state inside the vortex core. We then confirmed that the instability predicted in the linear equations was also present in the full GPE dynamics. Quite unexpectedly, we found that, while the instability is present at early times (and will cause the singularities to separate), the nonlinearity in the GPE pushes the two phase singularities back together once they reach a critical separation, resulting in a modulation of their separation. While it was already predicted that instabilities can be suppressed in certain trap geometries (e.g., [7,11]), it was not known that an unstable vortex state could do something besides decay into a well-separated pair of SQVs. The observed behavior exhibits qualitative similarities with sound reabsorption by solitons [22] and vortices [23], sound-mediated energy exchange between vortices in adjacent traps [24], and soliton trainlike behavior in superconductors following a quench [25,26].

The observed modulations of the separation between singularities are suggestive that, under the right conditions, corotating vortex pairs may be able to form metastable bound states. This surprising observation is reminiscent of the Berezinskii-Kosterlitz-Thouless phase transition [27], where vortices of opposite polarity form bound states below a critical temperature, although in our case the binding is a consequence of the trap geometry rather than the temperature. A

consequence is that our system never enters the regime where one can apply Hamiltonian vortex dynamics [21] since this requires that the vortex separation be much larger than the healing length. It would be interesting to see whether this behavior extends to more general scenarios, e.g., clusters of vortices. Although the resulting dynamics may be more complicated since there are more instabilities in the system (e.g., for $\ell = 3$ there are instabilities in the $m = 2, 3, 4$ modes [18]), we also expect these modulations to persist for higher winding numbers.

ACKNOWLEDGMENTS

S.P. would like to thank William G. Unruh for many stimulating discussions whilst this research was being conducted. S.P. acknowledges support from the Natural Science and Engineering Research Council (Grant No. 5-80441 to W. Unruh) and would also like to thank the IQSE, Texas A&M University, with grants from ONR (Award No. N00014-20-1-2184) and NSF (Grant No. PHY-2013771), for support and an intellectually stimulating environment while part of this work was done. C.F.B. and S.W. acknowledge support provided by the Science and Technology Facilities Council on Quantum Simulators for Fundamental Physics (ST/T00584X/1 and ST/T006900/1) as part of the Quantum Technologies for Fundamental Physics program. S.W. acknowledges support provided by the Leverhulme Research Leadership Award (Award No. RL-2019-020), the Royal Society University Research Fellowship (UF120112), and the Royal Society Enhancement Grant (Grant No. RGF/EA/180286) and partial support provided by the Science and Technology Facilities Council (Theory Consolidated Grant No. ST/P000703/1). A.G. and S.W. acknowledge support provided by the Royal Society Enhancement Grant (Grant No. RGF/EA/181015). S.E. and S.W. acknowledge support from the EPSRC Project Grant (Grant No. EP/P00637X/1). S.E. acknowledges partial support through Wiener Wissenschafts- und Technologie-Fonds (WWTF) Project No. MA16-066 ("SEQUEX") and support through an ESQ (Erwin Schrödinger Center for Quantum Science and Technology) fellowship funded through the European Union's Horizon 2020 research and innovation program under Marie Skłodowska-Curie Grant Agreement No. 801110. This project reflects only the authors' view, the EU Agency is not responsible for any use that may be made of the information it contains. ESQ has received funding from the Austrian Federal Ministry of Education, Science and Research (BMBWF).

APPENDIX A: SIMULATIONS

The numerical simulations of vortex decay presented in Fig. 2 are performed in three steps: (1) preparation of the initial state, (2) time evolution using the GPE (2), and (3) mode extraction.

For a given trap potential $V(r)$ of the form (3), the initial state is prepared by first estimating the lowest-energy configuration for a central $\ell = 2$ vortex. This is done by fixing the phase $\Psi \equiv \sqrt{\rho}e^{i\ell\theta}$ and evolving the modulus $\sqrt{\rho}$ in imaginary time $\tau \equiv it$, i.e.,

$$\partial_\tau \sqrt{\rho} = \left(\frac{1}{2}\partial_r^2 + \frac{1}{2r}\partial_r - \frac{\ell^2}{2r^2} - V(r) + 1 - \rho\right)\sqrt{\rho}. \quad \text{(A1)}$$

The resulting density ρ is inserted into a finite-difference matrix formulation of the BdG equation (5). Numerically solving for the eigenmodes and selecting the solution $|U\rangle = (u_+, u_-)^T$ with the largest imaginary part allows for the construction of the initial state,

$$\Psi_0 = e^{i\ell\theta}[\sqrt{\rho(r)} + \varepsilon u_+(r)e^{im\theta} + \varepsilon u_-^*(r)e^{-im\theta}]. \quad \text{(A2)}$$

Here $\varepsilon \ll 1$ is the initial amplitude of the unstable mode. For the data presented in Fig. 2, the values used are $\varepsilon = 10^{-3}$, $m = 2$, and $\ell = 2$.

The state Ψ_0 serves as the initial state for the full GPE simulation. Here the Cartesian plane is discretized into an $N \times N$ linearly spaced mesh of pixels with separation of Δl in each dimension. The time evolution proceeds in discrete time steps of duration Δt using a Fourier split operator method (see [28] for further details), which amounts to

$$\Psi(\mathbf{r}, t + \Delta t) \simeq e^{\frac{i\Delta t}{2}\nabla^2} e^{-i\Delta t(V - 1 + |\Psi|^2)}\Psi(\mathbf{r}, t). \quad \text{(A3)}$$

Provided that the boundary $x, y = \pm\frac{1}{2}(N-1)\Delta l$ of the simulation domain is well outside the potential boundary r_B, the wave function Ψ is sufficiently periodic for a Fourier-spectral evaluation of the exponentiated Laplacian in (A3). In the simulation presented in Fig. 2, the values $N = 768$, $\Delta l = 1/10$, and $\Delta t = 10^{-3}$ were used along with a potential of the form (2.2) with $a = 5$, $V_0 = 5$, and $r_B = 25$. Using the initial state and the discretization scheme outlined above, we perform $8\,192\,000 = 16\,384 \times 500$ time steps, of which every 500th frame is stored for later processing. The result is a collection $\Psi(x_i, y_j, t_k) \in \mathbb{C}^{N^2 \times N_t}$.

To extract the evolution of the unstable mode, the wave function $\Psi(x_i, y_j, t_k)$ is transformed to polar coordinates $\Psi(r_i, \theta_j, t_k)$ and Fourier transformed in the azimuthal direction to give $\Psi(r_i, m_j, t_k)$, where m_j is the jth azimuthal component. The imaginary part $\mathrm{Im}[\omega]$ of the frequency of the unstable mode is found by performing a log-linear fit to $|\Psi(r_i, m_j, t_k)|$ at $r_i = 1.5$ and $m_j = 2$. The real part $\mathrm{Re}[\omega]$ is computed (at the same points) using a temporal Fourier transform.

The energy

$$E = \int d^2\mathbf{x}\left(\underbrace{\frac{1}{2}|\nabla\sqrt{\rho}|^2}_{E_{\mathrm{qnt}}} + \underbrace{\frac{1}{2}|\sqrt{\rho}\nabla\Phi|^2}_{E_{\mathrm{kin}}} + \underbrace{V\rho}_{E_{\mathrm{pot}}} + \underbrace{\frac{1}{2}\rho^2}_{E_{\mathrm{int}}}\right) \quad \text{(A4)}$$

associated with a state $\Psi = \sqrt{\rho}e^{i\Phi}$ in the GPE may be decomposed into a quantum energy E_{qnt}, kinetic energy E_{kin}, trap energy E_{pot}, and interaction energy E_{int}. As first proposed by Nore *et al.* [20,29], the kinetic energy E_{kin} may be further split into a compressible part E_{kin}^c and an incompressible part E_{kin}^i. Defining $\mathbf{u} \equiv \sqrt{\rho}\nabla\Phi$ and introducing $\mathbf{u} \equiv \mathbf{u}_c + \mathbf{u}_i$ with $\nabla \cdot \mathbf{u}_i = 0$, the two components of the kinetic energy take the form $E_{\mathrm{kin}}^i = \int d^2\mathbf{x}\frac{1}{2}|\mathbf{u}_i|^2$ and $E_{\mathrm{kin}}^c = \int d^2\mathbf{x}\frac{1}{2}|\mathbf{u}_c|^2$. Numerically, such a decomposition may be obtained from the realization that if $\mathcal{F}$ denotes a spatial Fourier transform and $\mathbf{k}$

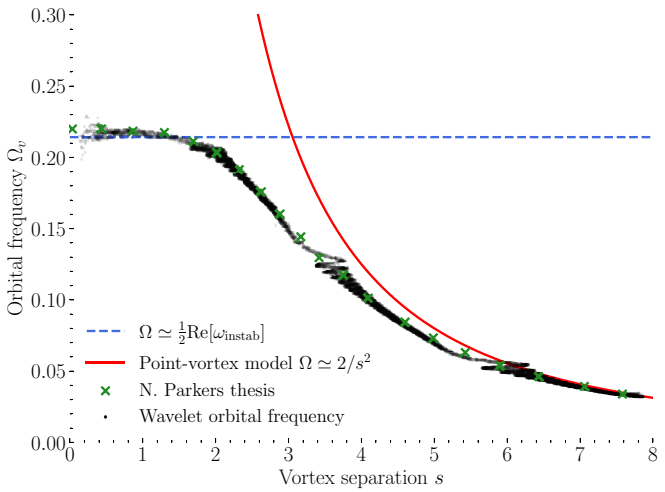

FIG. 4. The orbital frequency Ω of the two singularities as a function of the distance s between them (black line). At small s, the singularities are protovortices with Ω corresponding to the frequency of the unstable cavity mode (blue dashed line). At large s, the singularities are true vortices which obey the expected Hamiltonian point vortex dynamics (red line). We compare our data to a function used by Parker [32] (green crosses), who also considered the dynamics of nearby vortices.

denotes the corresponding wave vector, then $\mathbf{u}_c$ is nothing but the projection of $\mathbf{u}$ onto $\mathbf{k}$, i.e.,

$$\mathbf{u}_c = \mathcal{F}^{-1}\left[\frac{\mathbf{k}(\mathbf{k}\cdot\mathcal{F}\mathbf{u})}{|\mathbf{k}|^2}\right], \tag{A5}$$

where, in the absence of a mean flow, the $\mathbf{k} = 0$ component may be ignored to avoid zero division.

APPENDIX B: DAMPING

Dissipation is introduced in the GPE by using the phenomenological damping parameter γ [30,31],

$$i\partial_t\Psi = (1 - i\gamma)\big[-\tfrac{1}{2}\nabla^2 + V(\mathbf{x}) - 1 + |\Psi|^2\big]\Psi. \tag{B1}$$

The presence of dissipation damps out the oscillations of the two protovortices, which spiral away from each other and develop separate core regions. At this point we recover the well-known configuration of two point vortices of the same sign, which rotate around each other with an orbital frequency inversely proportional to the square of the vortex separation s, as shown in Fig. 4. The fact that the point vortex description predicts a divergence as $s \to 0$, signaling the breakdown of the model, is a consequence of the overlapping vortex cores. In this regime, the system is better described as a perturbation (cavity mode) on an $\ell = 2$ vortex background. This mode enters the linear regime in the limit $s \to 0$, and we see that the orbital frequency of the singularities tends to half of the oscillation frequency of the instability. The half is because two nearby singularities make a perturbation with $m = 2$; hence, it takes twice the time for a given peak of the $m = 2$ mode to return to its original position.

Another interesting feature of Fig. 4 is the sudden oscillations in s as the orbital frequency decreases. This occurs when the cavity mode reaches the correct frequency to couple to another phonon in the system. There are two such oscillations in Fig. 4 because at $r_B = 25$, there are two phonons with lower frequency than the cavity mode. Hence, for a small system where the cavity mode initially couples to the lowest phonon, these sudden additional oscillations would not occur.

In general, for the nonlinear modulations of the singularity pair to be observable in the presence of damping, the time taken for the singularities to spiral in and out should be shorter than the scale set by dissipation. Judging from Fig. 2(g) in the main text, the vortex spirals occur on a timescale of the order of $\mathrm{Im}[\omega]^{-1}$, where ω is the frequency of the unstable mode. Hence, the modulations should be observable provided $\gamma \ll \mathrm{Im}[\omega]$ is satisfied.

APPENDIX C: TWO-OSCILLATOR MODEL

The switch from exponential growth to decay observed in our simulations is characteristic of two oscillators (with opposite-sign energies) interacting under the influence of a nonlinearity. We illustrate this using a simplified model with the following Lagrangian:

$$\begin{aligned} L &= \tfrac{1}{2}\dot{\mathbf{X}}_+^2 - V_+ - \tfrac{1}{2}\dot{\mathbf{X}}_-^2 + V_- - g\mathbf{X}_+\cdot\mathbf{X}_-, \\ V_\pm &= \tfrac{1}{2}(\Omega^2 \pm \sigma)\mathbf{X}_\pm^2 - \tfrac{1}{4}c_\pm\mathbf{X}_\pm^4, \end{aligned} \tag{C1}$$

which describes two particles at $\mathbf{X}_\pm = (X_\pm, Y_\pm)$ oscillating about the coordinate origin with energies $H_\pm = \pm(\frac{1}{2}\dot{\mathbf{X}}_\pm^2 + V_\pm)$, respectively. The interaction energy between the two particles is $g\mathbf{X}_+\cdot\mathbf{X}_-$. We set $c_+ = 0$ and $c_- = \varepsilon > 0$ so that the nonlinearity affects only the particle located at $\mathbf{X}_-$.

To show that this model captures the essential features of the vortex evolution, we consider two limiting cases. When $g = 0$, the two particles oscillate at fixed radii as $\mathbf{X}_\pm \sim e^{-i\omega_\pm t}$ with frequencies $\omega_+ = \{\Omega^2 + \sigma\}^{\frac{1}{2}}$ and $\omega_- = \{\Omega^2 - \sigma - \varepsilon\mathbf{X}_-^2\}^{\frac{1}{2}}$. Here $\mathbf{X}_-$ mimics the way the orbital frequency of two point vortices decreases as the distance between them grows, while $\mathbf{X}_+$ mimics the phonon whose frequency (determined predominantly by the system size) stays nearly constant. Next, when $\varepsilon = 0$, both particles oscillate about the origin as a linear superposition of the frequencies $\omega = \{\Omega^2 \pm \sqrt{\sigma^2 - g^2}\}^{\frac{1}{2}}$. Notice that when the oscillator spacing is smaller than the coupling, $|\sigma| < |g|$, this will have unstable solutions, mimicking the behavior in Fig. 1 where instabilities occur if an $\mathcal{N} > 0$ mode comes close to an $\mathcal{N} < 0$ mode in the ω plane.

The full model with ε and g being nonzero has an elegant solution in the regime $\Omega \gg \sigma, g, \varepsilon\mathbf{X}_-^2$ (which is the relevant one for the vortex where $\mathrm{Re}[\omega]$ is an order of magnitude larger than $\mathrm{Im}[\omega]$). Defining the complex variable $Z_\pm = e^{i\Omega t}(X_\pm + iY_\pm)$ and rescaling such that $\Omega = 1$ and $\varepsilon = 2$, the Lagrangian becomes

$$\begin{aligned} L = \mathrm{Im}[Z_+\dot{Z}_+^* - Z_-\dot{Z}_-^*] - \tfrac{1}{2}\sigma(|Z_+|^2 + |Z_-|^2) \\ - g\mathrm{Re}[Z_+Z_-^*] - \tfrac{1}{2}|Z_-|^4. \end{aligned} \tag{C2}$$

This has a conserved charge $\mathcal{Q} = |Z_+|^2 - |Z_-|^2$ analogous to $\mathcal{N}$ for the vortex. For exponentially growing/decaying modes, this is conserved only when $\mathcal{Q} = 0$, implying $Z_\pm = |Z_\pm|e^{-i\varphi_\pm}$ with $|Z_\pm| = R$. In terms of R and the phase difference $\vartheta =$

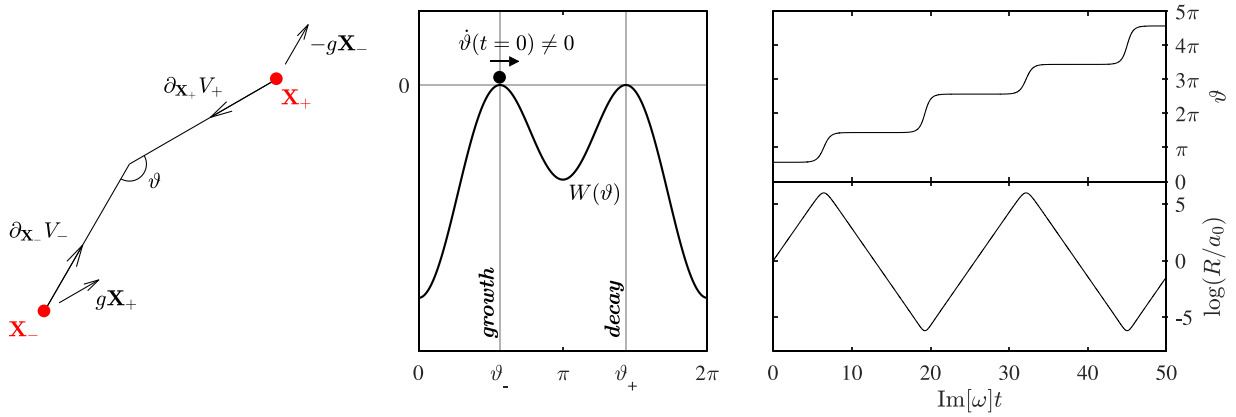

FIG. 5. Left: A schematic of the two interacting oscillators described by the Lagrangian (C1), where $\mathbf{X}_+$ represents a positive-energy phonon and $\mathbf{X}_-$ represents the negative-energy oscillation of the vortex (cavity mode). Middle: In the limit that the central oscillator frequency Ω is much larger than other scales in the problem, the dynamics can be reexpressed as a nonlinear oscillator ϑ moving through periodic potential W with two wells. Right: When ϑ evolves as it rolls along W, the original amplitude $R = |\mathbf{X}_\pm|$ switches between exponential growth and decay, mimicking the observed behavior in our simulations.

$\varphi_+ - \varphi_-$, we get

$$L = R^2\big(\dot{\vartheta} - \sigma - g\cos\vartheta - \tfrac{1}{2}R^2\big), \tag{C3}$$

which leads to the following equations of motion:

$$\dot{\vartheta} = \sigma + g\cos\vartheta + R^2, \quad \dot{R} = \tfrac{1}{2}gR\sin\vartheta. \tag{C4}$$

These can then be combined into a single equation for ϑ,

$$\ddot{\vartheta} + W'(\vartheta) = 0, \quad W(\vartheta) = -\tfrac{1}{2}(\sigma + g\cos\vartheta)^2, \tag{C5}$$

which describes a particle on $\mathbb{S}^1$ moving through a potential W. When the linear equations are unstable, W has two maxima, $\vartheta_\pm = \pi \pm \cos^{-1}(\sigma/g)$. By considering the phase of the solutions when $\varepsilon = 0$, one finds that the stationary solutions $\vartheta = \vartheta_-$ and $\vartheta = \vartheta_+$ correspond, respectively, to the linearly growing and decaying modes. However, in the nonlinear case, (C4) tells us that a nonzero initial amplitude in the instability means $\dot{\vartheta} \neq 0$, making ϑ roll all the way over the two peaks. Once $\vartheta(t)$ is known, the amplitude can be found by solving the equation in (C4) for $\dot{R}$,

$$R(t) \sim \exp\left(\frac{1}{2}\int g\sin\vartheta(t)dt\right), \tag{C6}$$

which tells us that R switches between exponentially growing and decaying solutions as ϑ changes by 2π. This behavior is illustrated in Fig. 5.

The key feature of this model that renders it so simple is that it contains only two interacting modes. This is what leads to the periodicity of the modulation in Fig. 5. When other modes are taken into account (i.e., the other ω and m modes around the vortex), energy can be dissipated into these channels, and we would expect these cycles to lose perfect periodicity. This imperfect periodicity appears to be what we see in Fig. 2 in the main text.

[1] R. P. Feynman, Application of quantum mechanics to liquid helium, Prog. Low Temp. Phys. **1**, 17 (1955).

[2] C. D. Andereck, J. Chalups, and W. L. Glaberson, Tkachenko Waves in Rotating Superfluid Helium, Phys. Rev. Lett. **44**, 33 (1980).

[3] I. Bloch, J. Dalibard, and W. Zwerger, Many-body physics with ultracold gases, Rev. Mod. Phys. **80**, 885 (2008).

[4] C. F. Barenghi, L. Skrbek, and K. R. Sreenivasan, Introduction to quantum turbulence, Proc. Natl. Acad. Sci. USA **111**, 4647 (2014).

[5] Y. Shin, M. Saba, M. Vengalattore, T. A. Pasquini, C. Sanner, A. E. Leanhardt, M. Prentiss, D. E. Pritchard, and W. Ketterle, Dynamical Instability of a Doubly Quantized Vortex in a Bose-Einstein Condensate, Phys. Rev. Lett. **93**, 160406 (2004).

[6] T. Isoshima, M. Okano, H. Yasuda, K. Kasa, J. A. M. Huhtamäki, M. Kumakura, and Y. Takahashi, Spontaneous Splitting of a Quadruply Charged Vortex, Phys. Rev. Lett. **99**, 200403 (2007).

[7] M. Okano, H. Yasuda, K. Kasa, M. Kumakura, and Y. Takahashi, Splitting of a quadruply quantized vortex in the Rb Bose-Einstein condensate, J. Low Temp. Phys. **148**, 447 (2007).

[8] C. F. Barenghi and N. G. Parker, *A Primer on Quantum Fluids* (Springer, Switzerland, 2016).

[9] H. Pu, C. K. Law, J. H. Eberly, and N. P. Bigelow, Coherent disintegration and stability of vortices in trapped Bose condensate, Phys. Rev. A **59**, 1533 (1999).

[10] T. Torres, S. Patrick, M. Richartz, and S. Weinfurtner, Analogue black hole spectroscopy; or how to listen to dumb holes, Class. Quantum Grav. **36**, 194002 (2019).

[11] L. Giacomelli and I. Carusotto, Ergoregion instabilities in rotating two-dimensional Bose-Einstein condensates: Perspectives on the stability of quantized vortices, Phys. Rev. Res. **2**, 033139 (2020).

[12] R. Brito, V. Cardoso, and P. Pani, *Superradiance* (Springer, Switzerland, 2020).

[13] T. Torres, S. Patrick, A. Coutant, M. Richartz, E. W. Tedford, and S. Weinfurtner, Rotational superradiant scattering in a vortex flow, Nat. Phys. **13**, 833 (2017).

[14] M. C. Braidotti, R. Prizia, C. Maitland, F. Marino, A. Prain, I. Starshynov, N. Westerberg, E. M. Wright, and D. Faccio, Measurement of Penrose Superradiance in a Photon Superfluid, Phys. Rev. Lett. **128**, 013901 (2022).

[15] S. R. Dolan, Instability of the massive Klein-Gordon field on the Kerr spacetime, Phys. Rev. D **76**, 084001 (2007).

[16] C. J. Pethick and H. Smith, *Bose–Einstein Condensation in Dilute Gases* (Cambridge University Press, Cambridge, 2008).

[17] M. V. Berry and K. Mount, Semiclassical approximations in wave mechanics, Rep. Prog. Phys. **35**, 315 (1972).

[18] S. Patrick, A. Geelmuyden, S. Erne, C. F. Barenghi, and S. Weinfurtner, Quantum vortex instability and black hole superradiance, Phys. Rev. Res. (to be published), arXiv:2112.12266.

[19] We have also confirmed that unstable modes are absent in the stable windows predicted by Fig. 1.

[20] C. Nore, M. Abid, and M. E. Brachet, Decaying Kolmogorov turbulence in a model of superflow, Phys. Fluids **9**, 2644 (1997).

[21] P. K. Newton and M. F. Platzer, N-vortex problem: Analytical techniques, Appl. Mech. Rev. **55**, B15 (2002).

[22] N. G. Parker, N. P. Proukakis, M. Leadbeater, and C. S. Adams, Soliton-Sound Interactions in Quasi-One-Dimensional Bose-Einstein Condensates, Phys. Rev. Lett. **90**, 220401 (2003).

[23] N. G. Parker, N. P. Proukakis, C. F. Barenghi, and C. S. Adams, Controlled Vortex-Sound Interactions in Atomic Bose-Einstein Condensates, Phys. Rev. Lett. **92**, 160403 (2004).

[24] N. G. Parker, A. J. Allen, C. F. Barenghi, and N. P. Proukakis, Coherent cross talk and parametric driving of matter-wave vortices, Phys. Rev. A **86**, 013631 (2012).

[25] R. A. Barankov, L. S. Levitov, and B. Z. Spivak, Collective Rabi Oscillations and Solitons in a Time-Dependent BCS Pairing Problem, Phys. Rev. Lett. **93**, 160401 (2004).

[26] E. A. Yuzbashyan, O. Tsyplyatyev, and B. L. Altshuler, Relaxation and Persistent Oscillations of the Order Parameter in Fermionic Condensates, Phys. Rev. Lett. **96**, 097005 (2006).

[27] J. M. Kosterlitz and D. J. Thouless, Ordering, metastability and phase transitions in two-dimensional systems, J. Phys. C **6**, 1181 (1973).

[28] J. Javanainen and J. Ruostekoski, Symbolic calculation in development of algorithms: Split-step methods for the Gross-Pitaevskii equation, J. Phys. A **39**, L179 (2006).

[29] C. Nore, M. Abid, and M. E. Brachet, Kolmogorov Turbulence in Low-Temperature Superflows, Phys. Rev. Lett. **78**, 3896 (1997).

[30] S. P. Cockburn and N. P. Proukakis, The stochastic Gross-Pitaevskii equation and some applications, Laser Phys. **19**, 558 (2009).

[31] N. P. Proukakis and B. Jackson, Finite-temperature models of Bose-Einstein condensation, J. Phys. B **41**, 203002 (2008).

[32] N. Parker, Numerical studies of vortices and dark solitons in atomic Bose-Einstein condensates, Ph.D. thesis, Durham University, 2004.